Unscented Kalman Filter Based State and Parameter Estimation in Percussive Drilling Systems

Xianfeng Song[1], Pascal-Alexandre Kane[2], Mohammad Ali Abooshahab[1]

1. Norwegian University of Science and Technology, Trondheim, Norway.
E-mail: xianfeng.song@ntnu.no

2. SINTEF Industry, Trondheim, Norway.

Abstract: Down-The-Hole (DTH) percussion tool is recognized for its high average rate of penetration (ROP), when drilling medium hard to very hard rock formations. This ROP which depends on the bit-rock contact conditions at the well bottom to efficiently transfer the impact energy to an intact rock can be maximized for certain parameter sets, including the static weight on bit (WOB, also known as thrust force/feed force). Indeed, recent experimental and numerical investigations of the bit-rock interface (BRI) have revealed an optimum WOB which is rooted in the dependence of the BRI law on the WOB force. That is an optimal state of pseudo-stiffness at the BRI can be obtained with the applied WOB for which the impact energy transmitted to rock is maximized. Therefore, accurate estimation and control of the BRI stiffness is crucial in order to optimize drilling operation. In this paper, a numerical solution is proposed which can estimate the state of drilling dynamics and evolving BRI stiffness. This approach combines a 1D phenomenological percussive drilling model accounting for the longitudinal wave transmission during bit-rock interaction and a joint Unscented Kalman Filter (UKF) designed to simultaneously estimate the unknown parameters in the nonlinear BRI stiffness expression as well as the inaccessible states at the BRI. The results show that this approach has the potential to provide an accurate estimation of the percussive drilling dynamics and nonlinear BRI stiffness evolution over a wide range of initial conditions and static deformations that induced from changing WOB.

Key Words: Percussive drilling, Unscented Kalman Filter, State estimation

1 Introduction

DTH percussive drilling tools today are extensively used for excavating hard rock formations, e.g. for mining applications and more recently for harvesting deep geothermal energy. Rock fragmentation in DTH drilling relies on the application of repeated impulsive loading, produced from hammer impacting on a rotated anvil/bit, to achieve the penetration in the rocks, schematically shown as Fig. 1.

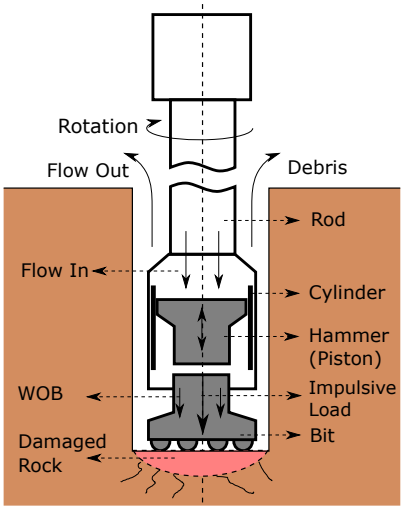

Fig. 1: Sketch of DTH percussive drilling system [1].

Although drilling with the pneumatic percussive tools is now a mature technology, which was introduced about one century ago [2], fundamental knowledge about the complex process of rock drilling is still lacking, including the rock fragmentation and bit/rock interaction [1]. Both laboratory and field tests have shown that the averaged ROP, the most important indicator for percussive drilling performance, can be maximized for certain parameter sets, including the WOB [3]. The root causes of the optimal drilling performance are still under discussion and need further understanding. Motivated by experimental evidence, recent theoretical research has revealed a nonlinear dependency of the BRI law with the applied WOB that can be correlated with the existence of an optimal WOB to maximize the impact energy transmission [1]. This is promising with respect to exploiting the model for advising drilling operations if further observations in percussive drilling tests can confirm the proposed hypothesis. Then the model can form the basis for model-based parameter identification and ROP optimization control algorithm running in real-time alongside the drilling operation [1]. Thus, a separate experimental program on percussive drilling is expected to investigate the stress/energy transmission efficiency given different WOB (BRI stiffness).

However, despite the advancement in sensor technologies, it is anticipated that this laboratory characterization and validation of the drilling dynamics is limited by various uncertainties in the course of bit-rock interactions, e.g. conspicuous mechanical vibrations and stress wave dispersion during the drilling process. In other words, the sequential measurements in percussive drilling are subjected to multiple disturbances, as shown in [3] where the transmitted forces obtained from the lateral strain gauge and rear force measurement produce approximately 30% deviation. Therefore, it is necessary to combine the experimental measurements with the mathematical representation of the drilling mechanical system to establish a good estimation of the true states around the BRI.

In case of constant stiffness of the BRI (linear force penetration relationship), such an estimation approach that relies on a limited number of measurements can be carried out by applying Kalman Filter (KF). However, it was shown that

This work is supported by Research Council of Norway.

the actual BRI stiffness is changing during penetration of the bit, see Fig. 2 and is directly affected by the evolving nonlinear rock damage response under percussive activation. The

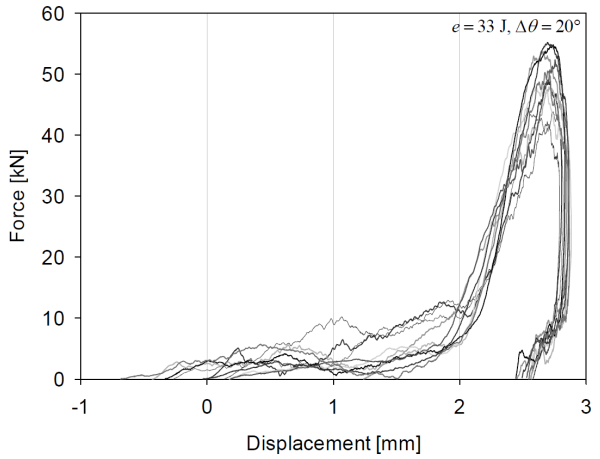

Fig. 2: Measured force versus penetration curves from drop tests [4].

most popular approach to address the nonlinear states estimation is the Extended Kalman Filter (EKF), which simply linearizes the nonlinear models so that the traditional linear KF can be applied [5]. Nevertheless, its performance is usually poor in presence of highly nonlinear transition as observed at the BRI under percussive impact. In order to overcome the limitations of EKF, other nonlinear state estimators have been proposed, including the UKF computational technique founded on the intuition that it is easier to approximate a probability distribution, rather than to approximate an arbitrary nonlinear function or transformation [5].

However, due to the overall complexity of harsh loading and environmental conditions underneath the bit buttons, accessible data of the percussive tool rock interaction response is usually restricted to the measurement on the side of the apparatus (while a strain gauge at the BRI will not resist to repeated impulsive load). Follow this paradigm, the estimation of the BRI state is performed in this study with the augmented UKF [6]. In this case, the unknown model parameters in the BRI stiffness expression are augmented in the state vector [7] and will be estimated by accounting for the presence of inherent disturbances expected at the BRI. In this paper, the noise production is assumed to follow a stochastic process accounting for the uncertainty of the data measured as well as the state model variables (which therefore accounting for the inherent discrepancies of the model).

The paper is organized as follows. In Section 2, we briefly describe the designed potential percussive drilling systems and associated system dynamics. Section 3 introduces the steps of implementing UKF. In Section 4, a representative analysis is presented, where the inaccessible BRI deformation and unknown BRI stiffness parameters are augmented with other states to be estimated simultaneously with UKF. Conclusions are drawn in Section 5.

2 Percussive Drilling Dynamics

A phenomenological model was recently proposed that qualitatively shows how the dependence of the pseudo-stiffness on the WOB influences the stress and energy transmission from the bit to the rock [1]. A separate experimental program is therefore required to validate the proposed hypothesis in order to exploit the model to instruct real-time control optimization.

In the designed potential percussive drilling experiments, a pre-indented rock specimen (for the purpose of generating craters with loose damages) will be used to investigate the stress and associated energy transmission efficiency given different WOB. To minimize the disturbances on determining the WOB impact on the stress/energy transmission, for instance from the frictional sliding of rock particles underneath drill buttons and the refinement of rock damages, the prepared craters have to be cleaned with air flushing in advance. Meanwhile, it is noted both in the static test and dynamic test that threshold energy exists below which no rock damage would be induced [8]. Therefore, the maximal driven impact energy will be restricted below this energy barrier, so that the effect from the growth of loose rock damages on BRI stiffness can be eliminated. In other words, the significant hysteresis loop induced by the rock fragmentation as shown in Fig. 2 will not be observed and the force-penetration response will primarily follow the same track given different WOB. Simon revealed in [9] that the efficiency of conversion of kinetic energy carried by the striking hammer into the potential energy/kinetic energy involved in the impulsive stress wave transmitted to the bit can be very high, as much as 100%. Therefore, for simplicity, the drill hammer will not be taken into account in this study. Instead, to achieve easy and accurate control of the input energy, percussive activation will be triggered by a controlled motion at the bit upper-bound, similarly to the apparatus presented in [10]. The vibro-impact system is used to drive the bit impacting the rock and its motion can be viewed as bounded oscillations around the bit upper boundary. Likewise, consider the uncertainties among different craters and shear effect on the BRI stiffness, bit indexing (rotation) will not be taken into account in this experimental study.

Accordingly, a phenomenological 1D representation de-

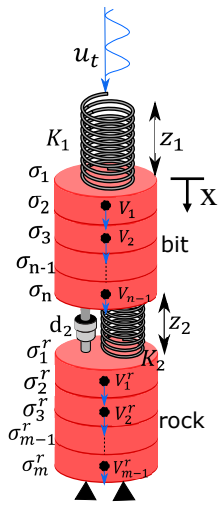

Fig. 3: 1D model for demonstrating the bit/rock interaction.

scribing the coupling among the bit, rock and BRI stiffness as in the drilling apparatus is proposed, see Fig. 3. The per-

cussive activation triggered by the impact hammer is controlled by the boundary displacement u_t. The model approximates the bit and rock as two finite elastic rods, where the displacement is constrained to zero at the rock bottom (rock specimen is mounted on a rigid ground). Moreover, in order to account for the contact conditions at the two interfaces (between the hammer/bit and bit/rock), two springs with stiffness equal to K_1 and K_2 respectively are used to approximate the contact deformation behavior. In addition, a damper with the coefficient d_2 is introduced at BRI, where the dissipation represents the absorbed impact energy without producing any rock fragmentation.

As shown in Fig. 3, bit and rock are discretized as $n-1$ and $m-1$ elements respectively to construct the numerical resolution. It is found that the motion of each body is primarily governed by the longitudinal wave equation that expresses the balance of linear momentum of an infinitesimal slice of the material,

$$\begin{cases} \dfrac{\partial V}{\partial t} = \dfrac{1}{\rho}\dfrac{\partial \sigma}{\partial x} \\ \dfrac{\partial \sigma}{\partial t} = E\dfrac{\partial V}{\partial x} \end{cases} \tag{1}$$

where ρ is the density, E is the Young's module, V is the particle velocity and σ is the stress.

The set of parameters can be reduced by reformulating the equations with dimensionless quantities. Correspondingly, the length of bit L_0 is chosen as the reference length scale. Consistency to the defined length scale, the time expense associated with wave traveling in bit is selected as the reference timescale $T = \frac{L_0\sqrt{\rho_1}}{\sqrt{E_1}}$. Thus the dimensionless time can then be defined as $\tau = \frac{t}{T}$. Additionally, the stress and velocity can be scaled as $\overline{\sigma} = \frac{\sigma}{E_1}$ and $\overline{V} = \frac{V\sqrt{\rho_1}}{\sqrt{E_1}}$. After introducing the scaled variables in the equation above, we can retrieve the law controlling the bit motion in a dimensionless form:

$$\begin{cases} \dfrac{\partial \overline{V}}{\partial \tau} = \dfrac{\partial \overline{\sigma}}{\partial \overline{x}} \\ \dfrac{\partial \overline{\sigma}}{\partial \tau} = \dfrac{\partial \overline{V}}{\partial \overline{x}} \end{cases} \tag{2}$$

Similarly the dimensionless dynamics of the rock can be written as:

$$\begin{cases} \dfrac{\partial \overline{V}^r}{\partial \tau} = \dfrac{\rho_1}{\rho_2}\dfrac{\partial \overline{\sigma}^r}{\partial \overline{x}} \\ \dfrac{\partial \overline{\sigma}^r}{\partial \tau} = \dfrac{E_2}{E_1}\dfrac{\partial \overline{V}^r}{\partial \overline{x}} \end{cases} \tag{3}$$

Note, in order to distinguish the movement between bit and rock in the system, the variables affixed with an additional superscript r are reserved for describing the rock dynamics. And parameters with subscript 1 and subscript 2 are used to represent the bit and the rock properties respectively.

The dynamics around the drill bit upper boundary can be obtained in terms of the rate of deformation and force balance,

$$\begin{cases} \dfrac{\partial \overline{Z}_1}{\partial \tau} = -\dfrac{\partial \overline{u}_t}{\partial \tau} + \overline{V}_1 \\ \overline{\sigma}_1 = \eta_1 \overline{Z}_1 \end{cases} \tag{4}$$

where $\overline{u}_t$ represents the prescribed non-dimensional bit upper bound motion, $\overline{V}_1$ and $\overline{\sigma}_1$ are the velocity and stress of the bit upper boundary respectively, and $\overline{Z}_1$ represents the dimensionless deformation of the impact interface between hammer and bit. For simplicity, the lumped parameter $\eta_1 = \frac{K_1 L_0}{E_1 A}$ is used to represent the dimensionless form of constant hammer-bit interface stiffness K_1.

Considering the other end of the bit, the original kinetic energy carried by the stress wave will be partly transmitted to the rock and be dissipated while the remaining portion will produce the high vibrations during bit/rock interactions. Given the force balance and rate of deformation at the BRI, the corresponding boundary conditions are characterized as:

$$\begin{cases} \dfrac{\partial \overline{Z}_2}{\partial \tau} = -\overline{V}_{n-1} + \overline{V}_1^r \\ \dfrac{\partial \overline{\sigma}_n}{\partial \tau} = \dfrac{\partial \overline{\sigma}_1^r}{\partial \tau} = \eta_2 \dfrac{\partial \overline{Z}_2}{\partial \tau} + \left(\dfrac{\partial \overline{V}_1^r}{\partial \tau} - \dfrac{\partial \overline{V}_{n-1}^r}{\partial \tau} \right) \overline{d}_2 \end{cases} \tag{5}$$

where $\overline{\sigma}_n$ and $\overline{\sigma}_1^r$ are the non-dimensional stress at BRI. $\overline{Z}_2$ refers to the inaccessible deformation at the BRI and $\eta_2 = \frac{K_2 L_0}{E_1 A}$ relates to the local dimensionless stiffness at the BRI. $\overline{d}_2$ is the dimensionless damping factor, which is given by $\frac{d_2}{L_0^2\sqrt{E_1\rho_1}}$. The stiffness K_2 between the two contact bodies is known to be nonlinear. In the context of percussive drilling, the nonlinear BRI pseudo-stiffness could be caused by an unknown combination of the loose debris underneath the bit buttons, changing bit-rock contact area, and crater volume expansion [1]. In order to approximate the nonlinearity of the BRI stiffness η_2, which is proved to increase along with the local deformation as illustrated in Fig. 2, it is presumed that the BRI stiffness follows an exponentially increase with the local deformation:

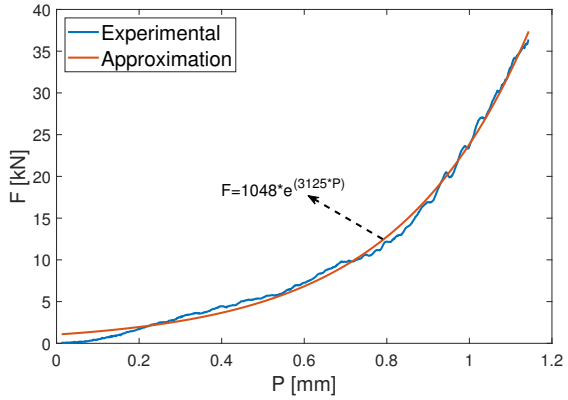

Fig. 4: Approximation of the force-penetration (F-P) response at BRI.

$$\eta_2 = \overline{\theta}_1 e^{\overline{\theta}_2(\overline{Z}_2 + \overline{Z}_{w0})} \tag{6}$$

where $\overline{\theta}_1$ and $\overline{\theta}_2$ are unknown parameters to be calibrated based on the online measurement. And $\overline{Z}_{w0}$ is the initial static deformation under the WOB. It is shown given the suggested stiffness expression at BRI, the corresponding BRI force-penetration approximation can give satisfactory precision when comparing to the response captured from the drop test in [4], see Fig. 4.

Given the fact that the rock specimen is mounted on the

rigid ground, the velocity is zero at the bottom of the rock specimen:

$$\overline{V}^{r}_{m-1} = 0 \tag{7}$$

Therefore, the residual stress wave in the rock will be the superposition of numerous partial transmissions and reflections. Conceivably, the drilling event will be influenced jointly by the BRI stiffness, frictional energy dissipation and elastic deformation of each component. Thus, accurately predicting the local BRI stiffness and associated BRI deformation is essential when determining the system response.

In a summary, the complete system can be given by the following nonlinear assemblies, described in a discrete form by using first-order Euler approximation:

$$\begin{cases}
\overline{V}_1(i+1) = \Big[\eta_1\left(\overline{\sigma}_2(i) + .. + \overline{\sigma}_{n-1}(i)\right) \\
\qquad + \dfrac{\eta_1}{\Delta\overline{x}}\left(\overline{Z}_2(i) + \overline{u}_t(i)\right) + \overline{\sigma}_2(i)\dfrac{1}{\Delta\overline{x}} \\
\qquad + \dfrac{\eta_1 E_1}{E_2}\left(\overline{\sigma}^r_2(i) + .. + \overline{\sigma}^r_{m-1}(i)\right)\Big]\Delta\tau + \overline{V}_1(i) \\
\overline{\sigma}_2(i+1) = \left[\dfrac{-\overline{V}_1(i) + \overline{V}_2(i)}{\Delta\overline{x}}\right]\Delta\tau + \overline{\sigma}_2(i) \\
\overline{V}_2(i+1) = \left[\dfrac{-\overline{\sigma}_2(i) + \overline{\sigma}_3(i)}{\Delta\overline{x}}\right]\Delta\tau + \overline{V}_2(i) \\
\qquad \vdots \\
\overline{V}_{n-1}(i+1) = \left[\dfrac{-\overline{\sigma}_{n-1}(i) + \overline{\sigma}_n(i)}{\Delta\overline{x}}\right]\Delta\tau + \overline{V}_{n-1}(i) \\
\overline{\sigma}_n(i+1) = \Delta\tau\Big[\overline{\theta}_1 e^{\overline{\theta}_2(\overline{Z}_2(i) + \overline{Z}_{w0}(i))}\left(\overline{V}^r_1(i) - \overline{V}_{n-1}(i)\right) \\
\quad + \overline{d}_2\left(\dfrac{\rho 1}{\rho 2}\dfrac{\overline{\sigma}^r_2(i) - \overline{\sigma}_n(i)}{\Delta\overline{x}} - \dfrac{\overline{\sigma}_n(i) - \overline{\sigma}_{n-1}(i)}{\Delta\overline{x}}\right)\Big] + \overline{\sigma}_n(i) \\
\overline{Z}_2(i+1) = \left[-\overline{V}_{n-1}(i) + \overline{V}^r_1(i)\right]\Delta\tau + \overline{Z}_2(i) \\
\overline{V}^r_1(i+1) = \dfrac{\rho_1}{\rho_2}\left[\dfrac{-\overline{\sigma}_n + \overline{\sigma}^r_2(i)}{\Delta\overline{x}}\right]\Delta\tau + \overline{V}^r_1(i) \\
\overline{\sigma}^r_2(i+1) = \dfrac{E_2}{E_1}\left[\dfrac{-\overline{V}^r_1(i) + \overline{V}^r_2(i)}{\Delta\overline{x}}\right]\Delta\tau + \overline{\sigma}^r_2(i) \\
\overline{V}^r_2(i+1) = \dfrac{\rho_1}{\rho_2}\left[\dfrac{-\overline{\sigma}^r_2(i) + \overline{\sigma}^r_3(i)}{\Delta\overline{x}}\right]\Delta\tau + \overline{V}^r_2(i) \\
\qquad \vdots \\
\overline{\sigma}^r_{m-1}(i+1) = \dfrac{-E_2\overline{V}^r_{m-2}(i)}{E_1\Delta\overline{x}}\Delta\tau + \overline{\sigma}^r_{m-1}(i) \\
\overline{\theta}_1(i+1) = \overline{\theta}_1(i) \\
\overline{\theta}_2(i+1) = \overline{\theta}_2(i)
\end{cases} \tag{8}$$

where $\Delta\tau$ is the chosen time step in the simulation. The time update for the augmented unknown parameters $\overline{\theta}_1$ and $\overline{\theta}_2$ allows no change beyond the effects of process noise since the parameters are defined to be constant.

3 Unscented Kalman Filter

UKF is known for its advantages over EKF, for instance, rapid convergence, ease of implementation and more accurate estimation. The fundamental component of UKF is to use a deterministic sampling technique, known as the unscented transform (UT), to pick a set of discretely sampled points (called sigma points) to parameterize the means and covariances of probability distributions [5]. A total of $2N+1$ weighted points will be derived from the augmented state and covariance matrix, and N is the dimension of the augmented state:

$$\begin{cases}
\chi^{[0]}_{k-1|k-1} = \mu_{k-1},\ for\, i = 1 \\
\chi^{[i]}_{k-1|k-1} = \mu_{k-1} + (\sqrt{(n+\lambda)\Sigma})_i,\ for\, i = 1, ..., N \\
\chi^{[i]}_{k-1|k-1} = \mu_{k-1} - (\sqrt{(n+\lambda)\Sigma})_{i-N}, \\
\qquad\qquad for\, i = N+1, ..., 2N
\end{cases} \tag{9}$$

where χ is the matrix of sigma points and $(\sqrt{(N+\lambda)\Sigma})_i$ is the i^{th} column of the matrix square root of $(N+\lambda)\Sigma$. The matrix square root can be calculated by using the numerically efficient and stable method Cholesky decomposition. λ is a scaling parameter defined as:

$$\lambda = \alpha^2(N+\kappa) - N \tag{10}$$

where α and κ are tuning parameters. The parameter $\alpha \in (0, 1]$ is used to adjust the spread of the sigma points.

Given the elaborately chosen sigma points, the filter first predicts the future state according to the developed process model. That is the sigma points are propagated through the nonlinear transition system, $\chi^{*[i]}_{k|k-1} = \mathcal{F}(\chi^{[i]}_{k-1|k-1})$, as Eq. (8) that derived for the percussive drilling system in this study. Note uncertainties, which are modeled as a stochastic process in this analysis, are assumed to be present not only in the measurements but also in the state dynamics. Then the propagated sigma points are weighted and recombined to produce the predicted mean $\overline{\mu}_k$ and covariance $\overline{\Sigma}_k$,

$$\begin{cases}
\overline{\mu}_k = \sum_{i=0}^{2N} w^{[i]}_m \chi^{*[i]}_{k|k-1} \\
\overline{\Sigma}_k = \sum_{i=0}^{2N} w^{[i]}_c [\chi^{*[i]}_{k|k-1} - \overline{\mu}_k][\chi^{*[i]}_{k|k-1} - \overline{\mu}_k]^T + R_k
\end{cases} \tag{11}$$

where the matrix R_k is the covariance of the transition noise. The corresponding weight w_m for the mean and the weight w_c for the covariance are given by:

$$\begin{cases}
w^{[0]}_m = \frac{\lambda}{n+\lambda},\ for\ i = 0 \\
w^{[0]}_c = w^{[0]}_m + (1 - \alpha^2 + \beta),\ for\ i = 0 \\
w^{[i]}_m = w^{[i]}_c = \frac{1}{2(n+\lambda)},\ for\ i = 1, ..., 2N
\end{cases} \tag{12}$$

where β is a non-negative weighting parameter introduced to affect the weighting of the zeroth sigma point for the calculation of the covariance [5]. Appropriate number for β depends accordingly of a specific problem, but a typical recommendation value is $\beta = 2$, which is optimal if states follow a true Gaussian distribution [5].

In the update phase, the prediction takes the current sensor measurements into account to refine the state estimation. Similar to the steps introduced above, a new set of $2N+1$ sigma points are derived from the mean and covariance,

$$\begin{cases}
\chi^{[0]}_{k|k-1} = \overline{\mu}_k,\ for\, i = 1 \\
\chi^{[i]}_{k|k-1} = \overline{\mu}_k + (\sqrt{(N+\lambda)\overline{\Sigma}_k})_i,\ for\, i = 1, ..., N \\
\chi^{[i]}_{k|k-1} = \overline{\mu}_k - (\sqrt{(N+\lambda)\overline{\Sigma}_k})_{i-N}, \\
\qquad\qquad for\, i = N+1, ..., 2N
\end{cases} \tag{13}$$

Transform these sigma points through the observation function $\mathcal{H}$ to compute the predicted measurements,

$$Z_{k|k-1} = \mathcal{H}(\chi^i_{k|k-1}), \quad for \quad i = 0, ..., 2N \tag{14}$$

Afterwards, the weighted sigma points are recombined to produce the predicted measurement and predicted measurement covariance.

$$\begin{cases} \hat{Z}_k = \sum_{i=0}^{2N} w_m^{[i]} Z_{k|k-1} \\ S_k = \sum_{i=0}^{2N} w_c^{[i]} (Z_{k|k-1}^{[i]} - \hat{Z}_k)(Z_{k|k-1}^{[i]} - \hat{Z}_k)^T + Q_k \end{cases} \tag{15}$$

where Q_k is the covariance matrix of the observation noise. Additionally, the state-measurement cross-covariance matrix is needed,

$$\overline{\Sigma}_k^{x,z} = \sum_{i=0}^{2N} w_c^{[i]} (\chi_{k|k-1}^{[i]} - \overline{\mu}_k)(Z_{k|k-1}^{[i]} - \hat{Z}_k)^T \tag{16}$$

to compute the UKF Kalman gain,

$$K_k = \overline{\Sigma}_k^{x,z} S_k^{-1} \tag{17}$$

Similar to the Kalman filter, the updated mean and covariance can be computed by including the Kalman gain,

$$\mu_k = \overline{\mu}_k + K_k(Z_k - \hat{Z}_k) \tag{18}$$

$$\Sigma_k = \overline{\Sigma}_k - K_k S_k K_k^T \tag{19}$$

4 Results

In this section, we consider the percussive drilling system illustrated as Fig. 3. The two objects are discretized as n-1 and m-1 elements respectively. For the demonstration purpose, we choose n=m=7 without losing the generality. The unknown parameter $\overline{\theta}_1$ and $\overline{\theta}_2$ are represented as additional elements of the state vector and simultaneously estimated in conjunction with other states. Therefore, the corresponding states (25 in total) of the researched system are: $\overline{V}_1, \overline{\sigma}_2, .., \overline{V}_6, \overline{\sigma}_7, \overline{Z}_2, \overline{V}_1^r, \overline{\sigma}_2^r, ..\overline{V}_5^r, \overline{\sigma}_6^r, \overline{\theta}_1$ and $\overline{\theta}_2$. In this simulation, the non-dimensional prescribed boundary motion is chosen as $\overline{u}_t = 0.001\left[\sin\left(2\pi\tau - \frac{\pi}{2}\right) + 1\right]$ and the system is assumed to be at rest before the perturbation.

Consider observation in this drilling system, states (stress and velocity) are usually directly observable apart from the inaccessible deformation at $\overline{Z}_2$ at BRI. Four states are selected to be measured by placing the sensors correspondingly on the side of bit and rock in the potential experiments: $\overline{\sigma}_4, \overline{V}_5, \overline{V}_3^r, \overline{\sigma}_5^r$. As the basis of constructing the simulation, the dimensionless parameter values used in the percussive drilling model and UKF are summarized in Table 1. The initial conditions for the states and parameters estimation are randomly chosen in the UKF estimation. Fig. 5 shows the stress $\overline{\sigma}_4$ estimation located in the middle of the bit. It can be seen that although given the noisy measurements, after a few steps, the estimated stress can spontaneously converge to the true states. Fig. 6 compared the estimated velocity of the fifth element $\overline{V}_5$ in the bit with its true states and measurements. In the case of predicting the dynamics in the rock, both the velocity and stress estimation are capable to obtain a track of the true state with high precision. The results are illustrated respectively in Fig. 7 and Fig. 8.

Table 1: Parameter Values

Parameter	Value	Parameter	Value
ρ_1	8000 $[kg/m^3]$	E_1	200 $[GPa]$
ρ_2	2700 $[kg/m^3]$	E_2	50 $[GPa]$
η_1	1	$\Delta\overline{x}$	1/6
$\overline{d}_2$	0.01	α	1
β	1	κ	0
$\overline{\theta}_1$	0.5	$\overline{\theta}_2$	-1

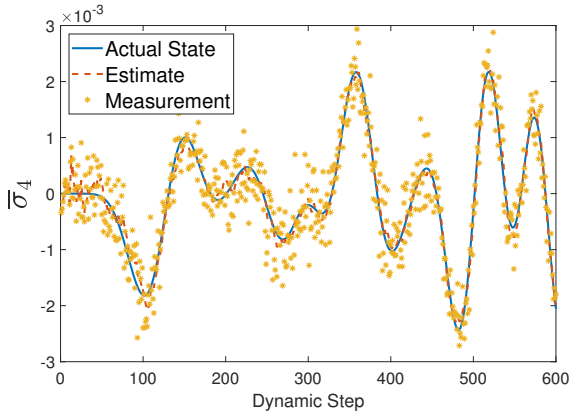

Fig. 5: Time step history of the stress $\overline{\sigma}_4$ obtained from UKF, compared to measurement and actual state.

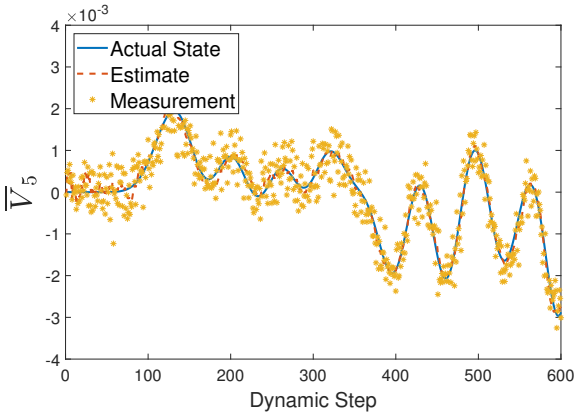

Fig. 6: Time step history of the velocity $\overline{V}_5$ obtained from UKF, compared to measurement and actual state

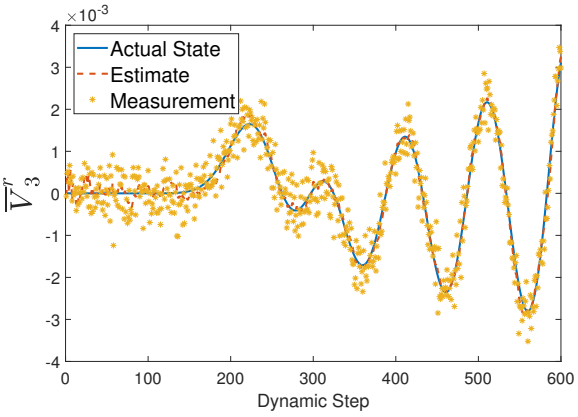

Fig. 7: Time step history of the velocity $\overline{V}_3^r$ obtained from UKF, compared to measurement and actual state.

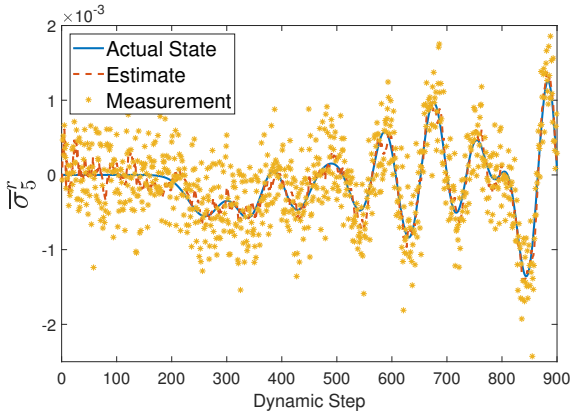

Fig. 8: Time step history of the stress $\overline{\sigma}_5^r$ obtained from UKF, compared to measurement and actual state.

Meanwhile, in particular, the estimation of the inaccessible deformation at BRI is shown in Fig. 9. Results show that

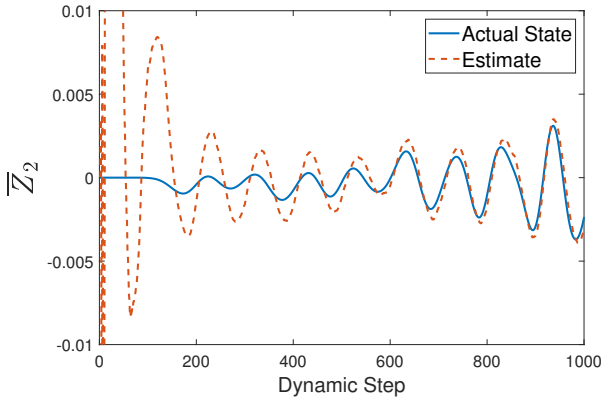

Fig. 9: Time step history of the deformation $\overline{Z}_2$ obtained from UKF, compared to measurement and actual state.

the UKF captures $\overline{Z}_2$ with high accuracy even missing the direct measurement of this state. Notably, it is necessary to verify the robustness of the nonlinear estimator in case of different initial conditions and operating conditions, where the changing WOB effect is considered by tuning static deformation $\overline{Z}_{w0}$ in step-wise alongside the simulation. It can

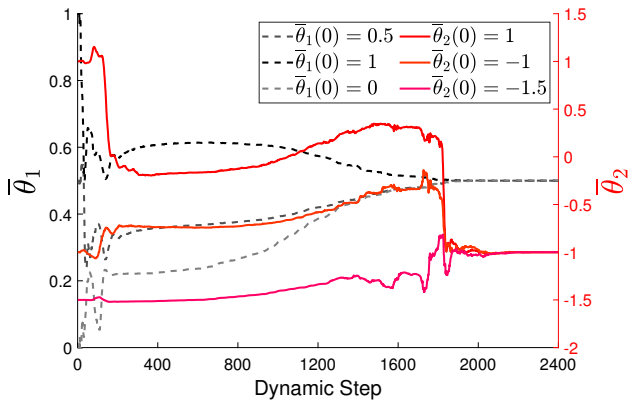

Fig. 10: Comparison of different initial conditions for $\overline{\theta}_1$ and $\overline{\theta}_2$ estimation.

be seen in Fig. 10 that for all the given initial conditions and changing static deformation, the unknown parameters $\overline{\theta}_1$ and $\overline{\theta}_2$ are able to converge to the true values eventually. It is speculated that the abrupt convergence of $\overline{\theta}_2$ to the true value is attributed to the nonlinear parameterization (until convergence of $\overline{\theta}_1$), which needs further investigation.

5 Conclusion

In this paper, a nonlinear dynamic model describing the designed potential laboratory DTH percussive drilling system is presented. Subjected to the anticipated pronounced disturbances in the measurements (e.g. vibrations, stress wave dispersion, etc.) and inaccessible state at BRI in the experiments, a joint Unscented Kalman filter is developed accordingly to simultaneously identify the true states and calibrate the unknown parameters in the BRI stiffness expression. The state estimation results obtained with the UKF are compared with the actual values and noisy measurement. It can be concluded although system dynamics incorporates with unknown parameters, the UKF can still be capable to obtain a satisfactory estimation of all states and reconstruct the parameter value accurately. This indicates that this approach has the potential to provide an accurate estimation of the DTH dynamics and nonlinear BRI stiffness evolution in the future test to investigate the WOB (BRI stiffness) impact on the stress/energy transmission.

References

[1] X. Song, A. Kane, O. Aamo, and E. Detournay, A dynamic model of the drilling action of percussive tools, in *53rd U.S. Rock Mechanics/ Geomechanics Symposium*, American Rock Mechanics Association, (NewYork), 2019.

[2] A. Muhammad, Control of ITH Percussive Longhole Drilling in Hard Rock, *McGill University, PhD Thesis* , 1996.

[3] W. Hustrulid and C. Fairhurst, A theoretical and experimental study of the percussive drilling of rock. *International Journal of Rock Mechanics and Mining Sciences* 1971;8:311-333, 335–356; 9(1972) 417–429, 431–449.

[4] M. Fourmeau, A. Depouhon, A. Kane, H. Hoang, and E. Detournay, Influence of indexation and impact energy on bit/rock interface law in percussive drilling: an experimental study. In *49th US Rock Mechanics/Geomechanics Symposium*, 2015, American Rock Mechanics Association.

[5] S. J. Julier and J. K. Uhlmann, Unscented filtering and nonlinear estimation, *Proceedings of the IEEE* **92**, pp. 401422, Mar 2004.

[6] E. Lourens, E. Reynders, G. D. Roeck, G. Degrande, and G. Lombaert, An augmented kalman filter for force identification in structural dynamics, *Mechanical Systems and Signal Processing* **27**, pp. 446 460, 2012.

[7] R. Furrer, M. G. Genton, and D. Nychka, Covariance tapering for interpolation of large spatial datasets, *Journal of Computational and Graphical Statistics* **15(3)**, pp. 502523, 2006.

[8] W. Hustrulid, A study of energy transfer to rock and prediction of drilling rates in percussive drilling, *University of Minnesota, Master Thesis* 1965.

[9] R. Simon, Transfer of the stress wave energy in the drill steel of a percussive drill to the rock, *International Journal of Rock Mechanics and Mining Sciences & Geomechanics Abstracts***1**, pp. 397411, May 1964.

[10] E. Pavlovskaia and M. Wiercigroch, Modeling of an impact system with a drift, *Physical Review E* **64**, pp. 1-9, 2001.